Cavitation Dynamics at Sub-Millimeter Scale

[1]Kunpeng Long, [2]Matevž Dular, [1,3]Olivier Coutier-Delgosha

[1]*Arts et Métiers ParisTech, Lille, France*
[2]*University of Ljubljana, Slovenia*
[3]*Virginia Tech, Kevin T. Crofton Aerospace and Ocean Engineering Dept., Blacksburg, VA, USA*

Abstract

This paper is focused on the dynamics of cloud cavitation at Sub-millimeter scales, between 0.1 and 10 mm. A simple flow configuration consisting in a small diameter jet impacting a wall at 90° and then flowing radially between two plates is used. Cavitation is obtained in the gap between the two plates, due to the local flow acceleration. The scale of the setup was changed by varying separately the gap between the two plates, and the nozzle diameter. Observations were performed from the transparent bottom plate, using a high-speed camera and intense illumination, for various Reynolds and cavitation numbers. The analysis is focused on the variations of the cavity length and the Strouhal number based on the characteristic frequency of the flow instability.

Keywords: Small Scale, cavitating flow, instability, flow imaging

1.Introduction

In the last decades, small-scale hydraulic systems have developed, due for example to new applications requiring small size underwater machines such as pipeline maintenance (Kim 2008) and urban underground or ocean engineering (Marani et al. 2009). In the medical area as well, the use of micro medical robots provides more secure, more accurate, and less invasive techniques for surgery (Kim et al. 2004). These small devices often involve high speed flows and/or low-pressure operation, which favors the development of cavitation. Although cavitating flows have been studied for a long time for various naval, nuclear or medical applications (to name only a few), there is almost no analysis in the literature of the scale effect on their structure and dynamics. However, the occurrence of scale effects on cavitation has long been known and was already mentioned by Ackeret in 1930. Numerous studies of scaling laws in cavitating flow were performed, but they all dealt with the problem of cavitation occurrence, while the case of fully developed cavitating flow was not considered (Holl *et al.* 1972; Arakeri & Acosta 1973; Gates & Billet 1980; Billet & Holl 1981; Ooi 1985; Amromin 2002). In addition, most of the studies have focused on large dimensions, typically between the cm and the meter, while Dular et al. (2012) have recently investigated the influence of lower scale (down to 3 mm) on cloud cavitation. In the later study, significant effects of the small size are reported, especially a damping of the unsteady effects at the smallest scales.

The objective of the present study is to extend this previous work to smaller scales, by analyzing the cavitation behavior for characteristic dimensions between 100 μm and 10 mm. Investigation of the flow at such small scale dramatically increases the complexity of the setup, especially to manufacture test sections with reliable dimensions, and the difficulty of investigation. Therefore, a very simple device, based on cavitation between two flat plates, has been used in the present study. Flow imaging with a high-speed camera has enabled to characterize various behaviors, according to the cavitation number, the Reynolds number and the scale of the setup.

2.Experiments Design and Setup

Cavitation tests were conducted in two small-scale cavitation tunnels at the University of Ljubljana (Slovenia) and Arts et Metiers ParisTech (Lille, France). The latter is schematically represented in figure 1.
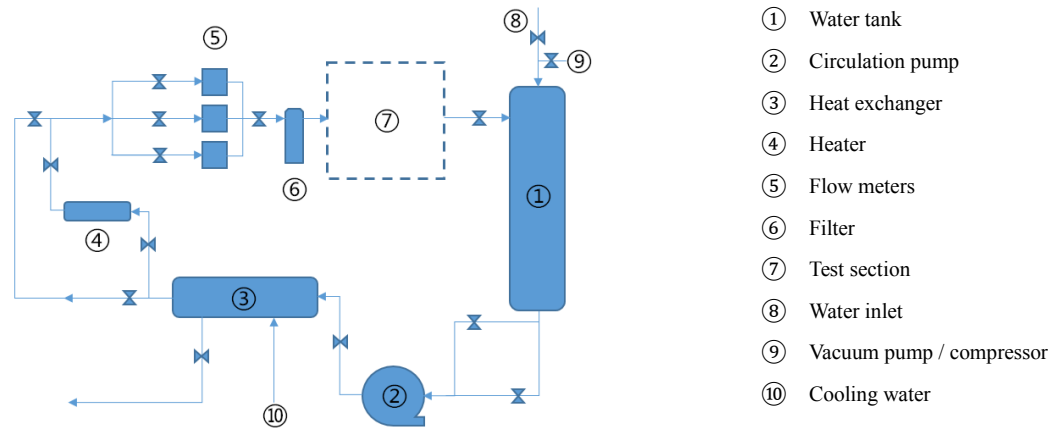

①	Water tank
②	Circulation pump
③	Heat exchanger
④	Heater
⑤	Flow meters
⑥	Filter
⑦	Test section
⑧	Water inlet
⑨	Vacuum pump / compressor
⑩	Cooling water

Figure 1. Cavitation tunnel at Arts et Metiers ParisTech

Circulation of water is obtained with a Salmson Multi HE 403 pump with variable rotation speed to set the flow rate. At the pump delivery, a tank completely filled with the circulation water is used for water cooling in order to maintain a constant temperature. The volume flow rate is measured a Bürkert type 8032 (uncertainty 0.15 l/min after in situ calibration) turbine flow meter for flow rates lower than 10 l/min and with a Bürkert type 8045 (2 % uncertainty) flow meter for higher flow rates. Temperature is obtained with a type K thermocouple, which is directly in contact with the circulation water. Upstream from the test section, a second tank partially filled with water is used to filter the flow rate and/or periodical pressure fluctuations due to the passage of the pump blades. The reference pressure is measured 30 mm upstream from the test section with a Rosemount 3051 pressure sensor. The uncertainty of the measurements was of the order of 10 mbar. The partially filled tank is connected to a compressor and a vacuum pump, which enables to vary the pressure in this tank between 0.1 bar and 3.5 bar, and thus to adjust the pressure in the test section.

Cavitation is obtained with a radial jet impacting a flat plate, as shown in Fig.2. The flow enters the test section at high velocity through a nozzle with a diameter D drilled in the upper plate. After it impact the bottom plate, a radial outward cavitating flow, between the bottom and upper plates is obtained. The gap between the two plates is denoted H. Cavitation is initiated slightly downstream from the edge of the inlet nozzle, and it collapses abruptly as the fluid moves radially outwards, since the pressure re-increases in the radial direction.
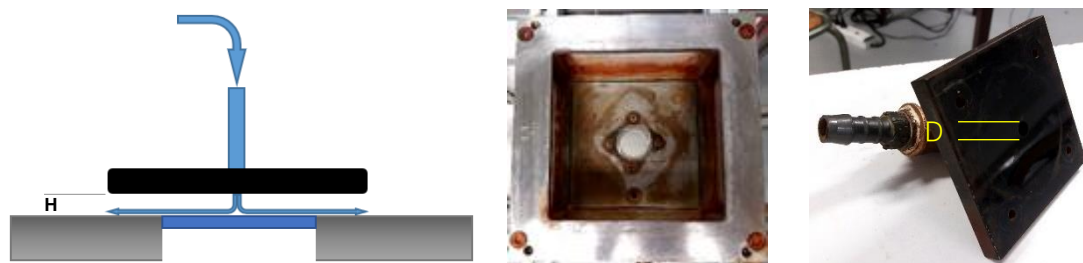

Figure 2. test section (a) scheme of the flow passage, (b) Top view of the bottom plate, (c) upper plate

A total of 13 geometrical configurations have been investigated, with a nozzle diameter varying between 1 and 10 mm and various gaps between the two plates, as indicated in table 1. Note that two experimental campaigns were

performed. In the data set#1 (cases A to F in table 1), a D = 3 mm diameter hole was mainly considered, with H varying between 0.1 mm and 1 mm. Two additional configurations with a bigger 10 mm hole diameter (H = 3 mm) and a smaller 1 mm diameter (H = 0.33 mm) were also studied to investigate the effect of the hole size. As reported in Section 3 hereafter, an abrupt change of cavitation behavior was detected between H = 0.3 mm and H = 0.7 mm, so a second experimental campaign was setup to investigate the transition between these two behaviors. In this 2nd set of experiments (cases G to M in table 1), holes of 3 mm and 6 mm diameter have been considered, for various values of H between 0.3 and 0.9 mm.

Geometry	D	H	D/H	Data Set
A	1	0.33	3.0	1
B	3	0.1	30.0	1
C	3	0.33	9.1	1
D	3	0.7	4.3	1
E	3	1	3.0	1
F	10	3.33	3.0	1
G	3	0.3	10.0	2
H	3	0.5	6.0	2
I	3	0.7	4.3	2
J	3	0.9	3.3	2
K	6	0.5	12.0	2
L	6	0.7	8.6	2
M	6	0.9	6.7	2

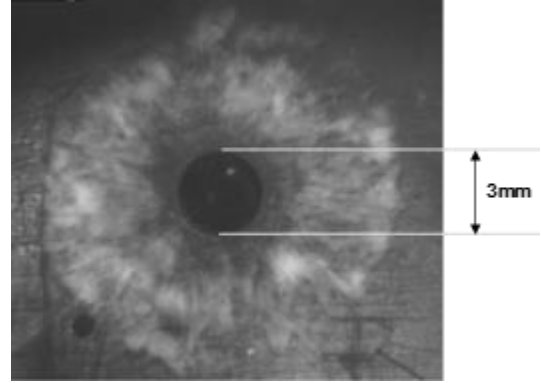Table 1. Investigated geometrical configurations

Figure 3. Example of cavitation in case J

A MotionBLITZ EoSens mini1 high speed camera is used for flow visualization from the bottom of the test section. Figure 3 presents the typical cavitation pattern obtained between the two plates. The maximum resolution of the camera is 1280×1024 pixels at 2000 fps, while it was used for the present tests at a higher frequency of 20K to 50K fps (depending on the frequency of cloud cavitation) with a typical resolution of 512×100 pixels. For that purpose, only a small band of cavitation was recorded at high frequency, instead of the whole axisymmetric cavitation pattern (see figure 4). In the second campaign, an optimization of the image quality was conducted, by testing 3 optics (Nikon AF nikkor 50mm, Nikon AF-S DX nikkor 40mm, and Nikon micro nikkor 105mm) combined extension rings and various continuous illumination sources. As a result, the contrast and the resolution of the image could be significantly improved for all data sets #2 (figure 4).
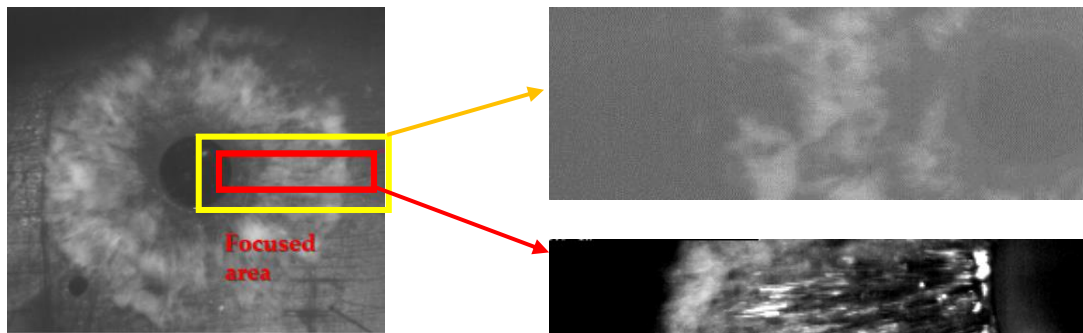

Figure 4. cavitation images (a) whole pattern, (b) zoom for high frequency acquisitions in data sets #1, (c) zoom in data sets #2

Various pressure and velocity conditions were investigated for each configuration, by varying the Reynolds number $Re = \frac{\rho v \cdot H}{\mu}$ and the cavitation number $\sigma = \frac{P - P_{vap}}{\frac{1}{2}\rho v^2}$.

Where v is the flow velocity between the plates at the nozzle radius and P is the inlet pressure measured upstream

from the injection nozzle. Post-processing of the images was performed with MATLAB. It basically consists in analyzing the grey level variations in the images to extract the mean cavity length L and the cavity oscillation frequency f. The cavity length is defined as the distance from the edge of the nozzle (location of cavitation inception) to the downstream end of the attached (non-fluctuating) cavitation area. For frequency analysis, FFTs of the mean grey level in 10 windows of interest (size 10×10 pixels by default) are calculated, as shown in figure 5a. These 10 FFTs are eventually superimposed as shown in figure 5b, to get the main and secondary frequencies. In case the results were unclear, the windows of interest were adjusted on a case by case basis to increase the intensity of the max. peaks in the FFTs.
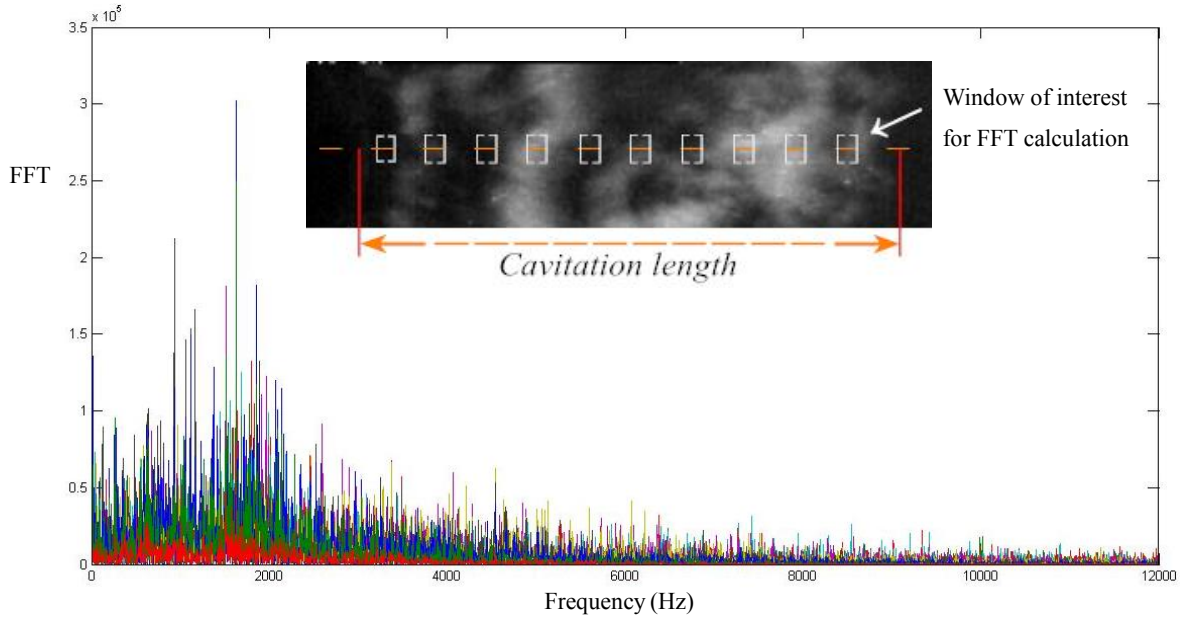

Figure 5. (a) Windows of interest for FFT calculation, (b) Superimposed 10 FFTs

3. Experimental results and discussion

The general cavitation behavior is similar in data sets 1 & 2. The axisymmetric cavitation cloud shows a periodic expansion and shrink in all experimental conditions (gap, diameter, and volume flow rate). In the results presented here, the Strouhal number $Str = \frac{f \times L}{v}$ is drawn according to $L_{norm} = \frac{L}{H}$. In figure 6, the results for data sets #1 (cases B to E) are drawn.
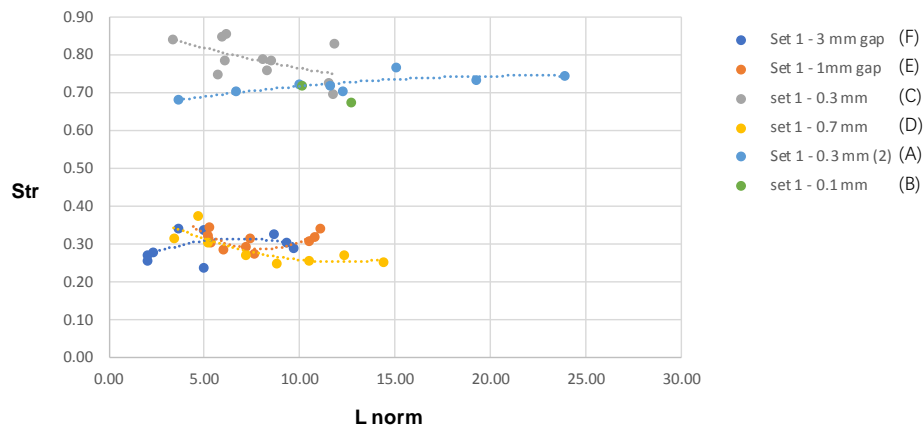

Figure 6. Variation of Str according to L_{norm} for the data sets #1

As mentioned previously, an abrupt modification of the flow behavior is obtained when H is decreased: for H higher or equal to 0.7 mm, the standard Strouhal number close to 0.3 is obtained, as usually reported in all studies of cloud cavitation at larger scale. So, it suggests that the flow dynamics is not influenced by the downscale of the geometry in such case. Conversely, when H is decreased down to 0.3 or lower, the Strouhal number becomes much higher, in the range 0.65 – 0.85. This significant and sudden change has motivated the second experimental campaign, where the objective was specially to investigate the transition from H = 0.7 mm down to 0.3 mm, and to determine which changes in the flow features could be responsible for this different unstable behavior.

Surprisingly, the results presented in figure 8 for data sets #2 look very different from the previous ones. Most of the values of the Strouhal number fall in the range 0.2 – 0.4 (for all geometrical configurations). No increase of the Strouhal number is observed when H is reduced down to 0.3 mm. Conversely, the Strouhal number increases up to 1.4 for very short sheet cavities in the specific case J where H = 0.9 mm and D = 3 mm. Generally, Str increases significantly for small values of L_{norm}. This specific behavior is related to the oscillation of very short cavities, where the characteristic frequency is hardly detectable, so it should be considered circumspectly here.
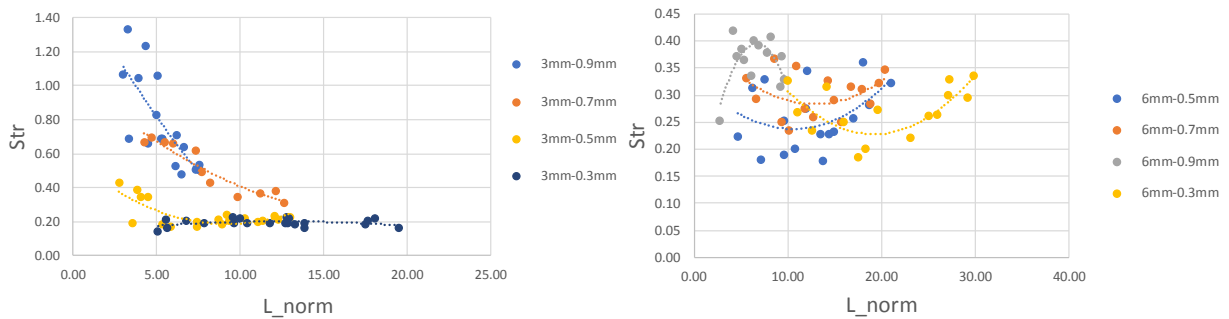

Figure 7. Strouhal number Str according to L_{norm} for cases G to M (data sets #2). In the caption, the first number refers to D and the second to H.

This difference between the two sets of data is highlighted in figure 8, which combines the results of both campaigns for the hole diameter D = 3 mm. The reason for this discrepancy is still currently investigated and the final results will be presented at the CAV 2018 conference. One possible explanation is related on some differences in the experimental process, between the two campaigns: in the first one, the Reynolds number was maintained constant and the cavity size was changed by varying the pressure with a vacuum pump and a compressor. In the second campaign, no pump was used, so the cavity size depends only on the flow velocity. A third experimental campaign is planned where a broader range of H and D values will be investigated.
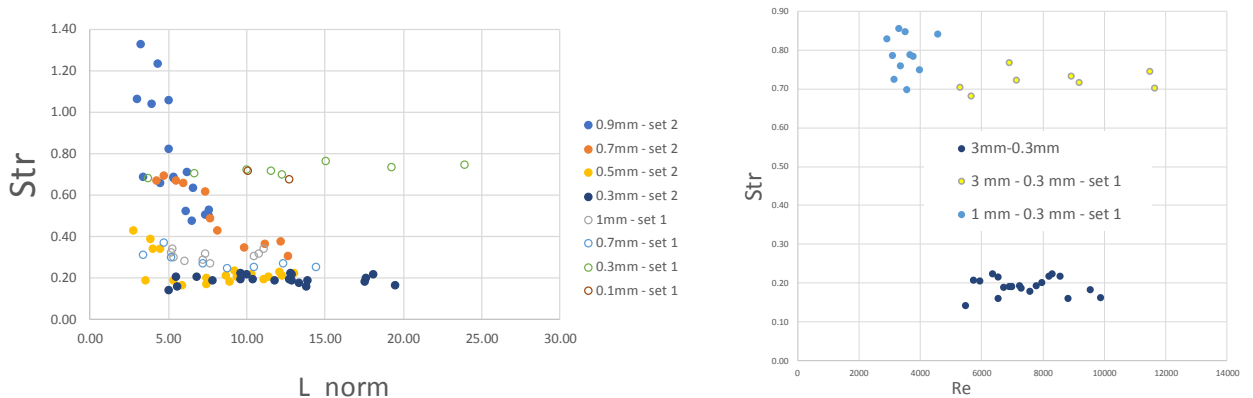

Figure 8. (a) comparison of the Strouhal number for the two sets of data and D = 3 mm, (b) Influence of the Reynolds number on the results for D = 3 mm and H = 0.3 mm

References

J. Ackeret (1930), Experimentelle und theoretische Untersuchungen über Hohlraumbildung (Kavitation) im Wasser. *Forschung im Ingenieurwesen* **1**(2), 63-72.

E. Amromin (2002) Scale Effect of Cavitation Inception on a 2D Eppler Hydrofoil. *J. Fluids Eng.* **124**(1), 186-193.

V.H. Arakeri, A.J. Acosta (1973), Viscous Effects in Inception of Cavitation on Axisymmetric Bodies. *J. Fluids Eng.* **95** (4), 519-526.

M.L. Billet, W. Holl (1981), Scale Effects on Various Types of Limited Cavitation. *J. Fluids Eng.* **103**(3), 405-414.

M. Dular, I. Khlifa, S. Fuzier, M. Adama Maiga, O. Coutier-Delgosha (2012), Scale effect on unsteady cloud cavitation, *Exp. Fluids* **53**, 1233-1250

E.M. Gates, M.L. Billet (1980), Cavitation Nuclei and Inception. IAHR Symposium, Tokyo, Japan.

J.W. Holl, R.E.A. Arndt, M.L. Billet (1972), Limited Cavitation and the Related Scale Effects Problem. The 2nd Int. JSME Symp. on Fluid Machinery and Fluidics, Tokyo, Japan.

B. Kim, Y. Jeong, T. Kim, J.O. Park, S. Song (2004), Micro capsule type robot, US Patent 6,719,684

J. H. Kim (2008), Design of a fully autonomous mobile pipeline exploration robot (FAMPER)

G. Marani, S. K. Choi, J. Yuh (2009), Underwater autonomous manipulation for intervention missions AUVs, *Ocean Engineering* **36**(1), 15-23

K.K. Ooi (1985), Scale effects on cavitation inception in submerged water jets: a new look. *J. Fluid Mech.* **151**, 367-390.